Simulation and Measurement Based Vehicle-to-Vehicle Channel Characterization: Accuracy and Constraint Analysis

Taimoor Abbas, *Member, IEEE,* Jörg Nuckelt, Thomas Kürner, *Senior Member, IEEE,* Thomas Zemen, *Senior Member, IEEE,* Christoph Mecklenbräuker, *Senior Member, IEEE,* and Fredrik Tufvesson, *Senior Member, IEEE*

***Abstract*—In this paper, a deterministic channel model for vehicle-to-vehicle (V2V) communication is compared against channel measurement results collected during a V2V channel measurement campaign using a channel sounder. Channel metrics such as channel gain, delay and Doppler spreads, eigenvalue distribution and antenna correlations are derived from the ray-tracing (RT) simulations as well as from the measurement data obtained from two different measurements in an urban four-way intersection. The channel metrics are compared separately for line-of-sight (LOS) and non-LOS (NLOS) situations. Most power contributions arise from the LOS component (if present) as well as from multipaths with single bounce reflections. Measurement and simulation results of the received power show a very good agreement in the presence of LOS, as most of the received power is carried by the LOS component. In NLOS, the difference is large because the ray-tracer is unable to capture some of the channel characteristics due to the underlying limitations of our ray-based propagation model. Despite the limitations, the model is suitable to characterize some, but not all, of the channel properties in a sufficient manner. We find that the diffuse scattering and multi-bounced non-specular reflections must be considered for an accurate prediction of the channel in such a rich scattering environment.**

I. Introduction

VEHICLE-TO-VEHICLE (V2V) communication has recently attracted considerable attention from both academia and vehicle industry as it facilitates cooperative driving among vehicles for improved safety, collision avoidance, and better traffic efficiency. The radio channel poses one of the main challenges for V2V communication system design because the V2V channel is highly dynamic. Fast variations in relative geometries, variable vehicle speeds and a number of different roadside environments - with a height of transmitter (TX) and receiver (RX) antennas relatively close to the ground level - makes the V2V channel significantly different from the well studied channels of other technologies such as cellular networks. Thus, a deep understanding of the underlying propagation channels is required.

In order to characterize V2V channel properties, a number of channel measurements and ray-tracing simulation-based studies have been presented in recent years, e.g., [1]–[9]. In addition to that, a large body of work on statistical channel modeling with measurement verification has been conducted in the past [10], [11]. Despite these efforts, there is still a need for adequate, reliable, deterministic and stochastic channel models facilitating realistic V2V system analysis [2], [12].

The measurement based investigations require a lot of effort and are costly in contrast to the deterministic model based ray-tracing simulations, which allow for investigation of any desired scenario with less effort and reduced complexity. However, the results obtained from the ray-tracing simulations strongly depend on the implemented mathematical models as well as on the accuracy of the data used to describe the environment. Thus, it is necessary to validate the simulations. Most of the measurement and simulation studies in the past have almost exclusively been performed independently except in a few cases [7], [13], [14]. This study is an extension of the work presented in [14], in which the simulation results obtained using a ray-optical model were compared against the results obtained from the DRIVEWAY channel measurements performed in the city of Lund, Sweden using the RUSK Lund channel sounder [4]. The ray-tracing simulator is developed by the researchers at TU Braunschweig, especially for vehicular communications in the $5.9\,$GHz band [5]. The simulations were done for the same urban intersections as where the measurements were performed. In [14], the analysis was limited to a single-input single-output (SISO) antenna configuration and a comparison was made only in terms of power delay profile (PDP) and path loss metrics.

The importance of an urban street intersection scenario is that the line-of-sight (LOS) path is often obstructed by surrounding buildings, which strongly limits the wave propagation and affects the link reliability in a negative way. In such a scenario the communication is highly dependent on the availability and strength of reflected multipath components (MPCs), which in turn depend on the location of the scatterers, material properties, street width, distance of the TX/RX to the intersection, and lateral distance of the transmitting node to surrounding buildings. Some path loss models have been derived to characterize such scenarios [6], [16] and were

T. Abbas and F. Tufvesson are with the Dept. of Electrical and Information Technology, Lund University, Lund, Sweden. e-mail: (taimoor.abbas@gmail.com, fredrik.tufvesson@eit.lth.se).

J. Nuckelt and T. Kürner are with Institut für Nachrichtentechnik, Technische Universität Braunschweig, Braunschweig, Germany. e-mail: (nuckelt, kuerner@ifn.ing.tu-bs.de).

C. Mecklenbräuker is with Institut für Nachrichtentechnik und Hochfrequenztechnik, Technische Universität Wien, Vienna, Austria. e-mail: (christoph.mecklenbraeuker@tuwien.ac.at).

Thomas Zemen is with AIT Austrian Institute of Technology, Vienna, Austria. e-mail: (thomas.zemen@ait.ac.at).

(a) (b) (c)

Fig. 1. (a) Google Earth™ [15] aerial image of the investigated urban crossroads scenario in the city of Lund with two vehicles moving towards the intersection at a speed of approximately $10\,\mathrm{m/s}$ (N55° 42′ 37″, E13° 11′ 15″). (b) and (c) show the perspective from the receiving vehicle RX-M1 and TX-M1, respectively.

validated using channel measurement data [17]. Both models assume an intersection with perpendicular crossings and cannot be applied directly to those with irregular geometries. Hence, urban intersections constitute an interesting scenario to investigate wherein a flexible semi-deterministic channel model for V2V communications is still required.

The main contribution of this work is a detailed evaluation of V2V channel parameters that is done by comparing the results obtained from the ray-tracing simulations and measurements for a 4×4 multiple-input multiple-output (MIMO) configuration in a four-way urban street intersection scenario. This paper is a sustained continuation of the work presented in [14], where channel metrics like PDP, channel gain and delay spreads have been analyzed for one V2V scenario. In addition to that, channel metrics like Doppler spreads, eigenvalue distribution, and MIMO diversity (which are related to the time-variant nature of the channel and to multi-antenna system) are derived. The measurement data is analyzed separately for both LOS and NLOS situations, where means and standard deviations of the errors are provided individually for each of the channel metrics, for two different TX and RX configurations. With the help of these channel metrics, the accuracy of the ray-tracing tool is analyzed and possible flaws or limitations of the underlying channel models are identified.

The remainder of the paper is organized as follows: Section II describes the measured urban intersection scenario as well as the different configurations of the TX and RX vehicles used during the measurements. Section III describes the RUSK-Lund channel sounder and the measurement setup. In section IV the ray-optical channel model used for the simulations is described. The channel measurement data and the simulation data are compared and analyzed in section V. Finally, in section VI the discussion is summarized and conclusions are presented.

II. Urban Intersection Scenario

For the comparison of simulation results against measurement data, we have chosen an urban four-way intersection (N55° 42′ 37″, E13° 11′ 15″, see Fig. 1(a)) in the city of Lund, Sweden. The scenario is exactly the same as the narrow urban scenario described in [18].

Two measurements have been selected for the analysis: M1) when the TX and RX cars are driving from the streets TX-M1 and RX-M1, and M2) when the TX and RX cars are driving from the streets TX-M2 and RX-M2, respectively, towards the intersection at a speed of approximately $10\,\mathrm{m/s}$. The photographs in Fig. 1(b) and Fig. 1(c) show a view from the RX vehicle of the the street RX-M1 and the TX vehicle of the street TX-M1, respectively. The line-of-sight (LOS) component was obstructed by four-story buildings located along each leg of the intersection. The four side roads are not perfectly perpendicular and the canyons of the streets are quite narrow, ranging from $14-17\,\mathrm{m}$. During the measurements there were parked vehicles along both sides of the streets. Furthermore, there were some traffic signs and lamp posts in the immediate environment of the intersection. There were doors, windows, and balconies with large metallic frames on the walls of the buildings, which give rise to stronger multipath components in comparison to plain concrete walls. It is worth mentioning that in M1 a bus is driving in front of the RX and turns left from the RX-M1 street to the TX-M1 street towards the west at the beginning of the scenario.

III. Channel Measurement Setup

The RUSK Lund channel sounder, which performs MIMO measurements based on the switched array principle, was used to record the complex time-varying channel transfer function $\mathbf{H}(f,t) \in \mathbb{C}^{M_R \times M_T}$, where M_T and M_R denote the number of transmit and receive antennas, respectively. The corresponding channel impulse response (CIR), $\mathbf{h}(\tau,t)$, is derived from $\mathbf{H}(f,t)$ by applying a Hann window to suppress side lobes and then an inverse Fourier transform is performed. For each measurement the sounder sampled the channel for $10\,\mathrm{s}$ - using a time increment of $\Delta t = 307.2\,\mu s$ it recorded $N_t = 33500$ time snapshots - over a bandwidth of $240\,\mathrm{MHz}$ at $5.6\,\mathrm{GHz}$ carrier frequency. Two regular hatchback cars with a height of $1.73\,\mathrm{m}$ and each equipped with a four-element antenna array were used to perform V2V measurements. Each antenna element in the array had a somewhat directional beam pattern pointing; 1) left, 2) back, 3) front, and 4) right, respectively. These antenna arrays, integrated into the existing radomes ('shark fins') on the car roof, were specifically designed for V2V communications [19]. The interested reader is referred to [4], where a detailed description of the measurement setup can be found.

IV. 3D Ray-optical Channel Model

The radio channel of the V2V scenario described above is characterized by utilizing a deterministic propagation model based on the ray-tracing principle [20]. The ray-based model has been specifically designed for the analysis of V2V communication scenarios [5], [21]. It includes a full 3-dimensional (3D) representation of the wave propagation and comprises the full-polarimetric antenna gain patterns of the TX and the RX, respectively. Several radio propagation mechanisms are taken into account to properly model the multipath nature of V2V channels. First of all, the LOS path between the TX and RX – if not obstructed by obstacles like buildings – is calculated based on the distance between both nodes and the free-space path loss formula. Scattering caused by surrounding objects is modeled in two different ways. On the one hand, specular reflections where the angles of the incident ray and the reflected ray are the same, are calculated by solving the well-known Fresnel equations. The corresponding reflection points are obtained by applying the image method [20]. Note that multi bounce interactions can be theoretically considered up to the n-th order in the case of specular reflections. However, for reasons of computational complexity the order of specular reflections is practically limited to three or four depending on the complexity of the investigated scenario. On the other hand, scattering in terms of non-specular reflections, i.e., diffuse scattering, is simulated by applying the Lambert's emission law [22]. The surface of an object that can be seen by both TX and RX is segmented into small tiles and, afterward, for each tile a single scattering process is solved according to the Lambert's emission law in order to obtain the corresponding scattering coefficients. It is worth mentioning that the current implementation of diffuse scattering accounts for single bounce interactions only. As it is shown later, this is a major limitation of the model when characterizing the V2V channel in such scattering rich urban street canyons.

Furthermore, from the authors' point of view it seems reasonable to neglect the contributions of diffracted waves in many cases at a frequency of 5.9 GHz, e.g., diffraction over the roof-top with large propagation distances. However, diffraction around the corners of the buildings and around large vehicles influence the received power especially when the TX/RX separation is below 100 m [23]. The current propagation model does not include diffraction, which is another limitation of the model.

In order to characterize the V2V radio channel using the ray-based model, the investigated scenario has to be described in detail, including all buildings and obstacles that mainly interact with the transmitted signal and, therefore, affect the wave propagation. For the analysis presented in this manuscript, building data for the design of a virtual scenario is obtained from OpenStreetMap (OSM).[1] In [24], a guideline and a proof-of-concept how to make use of OSM building data for 3D ray-tracing simulations is presented. The current development status of the database provides a detailed description of the buildings in metropolitan areas. Note that OSM usually provides only rare information about the individual height of buildings. However, the accurate building height is not essential in this peer-to-peer scenario as most of the wave propagation takes place at street level. For this reason, we have set the height of all buildings in this analysis to 15 m, which is close to the real height of these four- to five-story buildings along the roadside in this scenario. For the simulations, the faces of each building are assumed to be planar concrete surfaces with a single reflection coefficient, and the effects of metallic doors, windows and balconies have not been taken in to account, which is another constraint of the simulation setup compared to the real-world scenario.

By analyzing videos captured during the measurements and on-site inspections of the intersection, we identify relevant obstacles like traffic signs, lamp posts or parked cars along the roadside and add these objects in a simplified manner to the virtual scenario. Moreover, the positions of the moving TX and RX are reproduced using the GPS coordinates logged during the measurement runs. A time resolution of 10 ms has been chosen to initially sample the virtual scenario. For each snapshot the ray-based model determines the propagation paths (rays) including its electromagnetic properties. Depending on the number of rays, the computation time (accounting for multi-bounce specular reflections of order three) for one snapshot is in the range from a few milliseconds up to ten seconds using a standard desktop personal computer.

To further increase the time resolution of the sampled radio channel, the individual rays obtained from the ray-based models are interpolated in a post-processing routine [25] that is applied afterward. For the interpolation the information about the geometry of the close vicinity is exploited, i.e., the knowledge about the time evolution of the propagation paths that are determined by the ray-based model makes it possible to derive the ray information between any two adjacent snapshots. In this way, the time resolution of the sampled scenario is decreased to 100 μs enabling an adequate modeling of the Doppler effect. The intermediate result is a set of rays for each snapshot of the V2V scenario, illustrated in Fig. 2 as an example.

After a coherent superposition of all determined rays, the final output of the ray-based model is the time-variant CIR $\mathbf{h}(\tau, t) \in \mathbb{C}^{M_R \times M_T}$, which completely characterizes the frequency-selective channel for each TX/RX link. We can express the CIR as

$$\mathbf{h}(\tau, t) = \sum_{k=1}^{N(t)} a_k(t) \cdot e^{j(2\pi f \tau_k(t) + \varphi_k(t))} \cdot \delta(\tau - \tau_k) \tag{1}$$

$$= \sum_{k=1}^{N(t)} \tilde{a}_k(t) \cdot \delta(\tau - \tau_k), \tag{2}$$

[1] See www.openstreetmap.org

where the k-th multipath component is described by the amplitude $a_k(t)$, the delay $\tau_k(t)$ and the phase shift $\varphi_k(t)$ at time t. $N(t)$ and f denote the number of multipath components for each time instant and the carrier frequency of the system, respectively. Based on the predicted CIR, additional metrics like the PDP, channel again, RMS delay spread and so forth can be derived and compared with the measurement-based data.

V. Analysis

The main objective of this paper is to perform a validation of the ray-tracing simulation results, under some limitations, for the V2X channel by means of a comparison with measured channel data. In the simulations, we have restricted specular reflections to second order to keep the computational complexity low. Moreover, non-specular reflections of an order higher than one, diffuse scattering and diffraction components are not included. Given these restrictions and limitations, the goal is to find out how well the channel properties can be described using ray-tracing simulations under these simplified conditions. The signal reception is significantly different in LOS and NLOS situations, thus we characterize the channel metrics separately for LOS and NLOS situations.

A. Power Delay Profile and Doppler Spectral Density

The time-variant averaged power delay profile (APDP) is calculated by using the 4×4 MIMO channel transfer functions $H(t_k, f)$ obtained at time instants $t_k \;\forall\; k = 0, 1, ..., N_t$ from the measurement data as well as from the simulations as follows,

$$\mathbf{P}_\tau(t_k, \tau) = \frac{1}{N_{avg}} \sum_{n=0}^{N_{avg}-1} |\mathbf{h}(t_k + n\Delta t, \tau)|^2, \tag{3}$$

where the $\mathbf{P}_\tau(t_k, \tau) \in \mathbb{R}^{M_R \times M_T}$ is averaged over a window of N_{avg} time snap-shots such that $N_{avg}\Delta t = 57\,\text{ms}$ corresponding to a TX/RX movement of about 10 wavelengths at a speed of approximately $10\,\text{m/s}$. Furthermore, the processing includes noise reduction of the measurement data as described in [18].

The resulting APDP of the measurements and the simulations are depicted in Fig. 3(a) and 3(c) for M1 and in Fig. 3(b) and 3(d) for M2. At first sight, we find a good agreement when comparing the simulated APDP against the measurement data. Several MPC can be identified in both figures. However, there are individual discrete scatterers as well as diffuse scatterers that can be found in the measured APDP but not in the simulated one and vice versa.

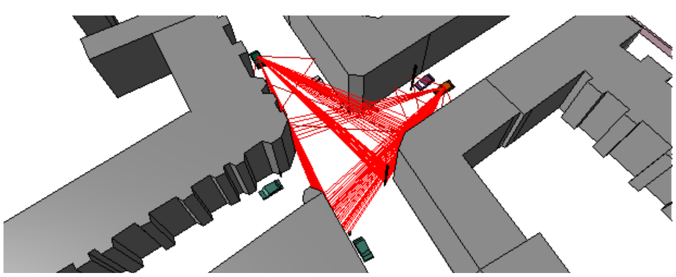

Fig. 2. Simulation of the underlying urban intersection scenario by means of ray-tracing. The data of the environment includes buildings, traffic signs, lamp posts as well as parked cars along the roadside.

In the first few seconds the TX and RX were far from the street intersection and the LOS between them was blocked by the buildings in both scenarios, the LOS components (C) and (F) appear at approximately $6.8\,\text{s}$ and $7.9\,\text{s}$ in M1 and M2, respectively. The number of MPCs originating from discrete as well as diffuse scatterers in the measured APDP is much higher than in the simulated APDP because of the incomplete building data. Moreover, in the simulations MPCs with first and second order reflections are considered only. In urban environments reflections of much higher order, up to 12, may exist as shown in [26]. However, the reflections with order higher than two in LOS and four in NLOS do not have significant contribution to the received power at $5.9\,\text{GHz}$ as shown in [14].

The groups of arrows (D) and (G) in Fig. 3 point at several specular and non-specular MPCs that possibly originate from nearby buildings and are captured in measurements as well as in simulations. There are power contributions (E) and (H) originating from the same building which has a metallic sheet on its walls but it does not act as perfect metallic surface in reality. However, in the simulations that building is considered as a metallic object which results in a slightly higher power contribution in contrast to the measurements for that component. This example, and other similar cases points to the need for a very detailed description of the environment if one aims for an almost ideal match between measurements and simulations.

B. Channel Gain

Based on the APDP, we calculate the time-variant channel gain, which includes the impact of the antennas used and front-end loss, as

$$\mathbf{G}(t_k) = \sum_\tau \mathbf{P}_\tau(t_k, \tau). \tag{4}$$

However, for the measured channel gain the impact of noise has been reduced by setting any component below the noise threshold plus $3\,\text{dB}$ to zero in the APDPs. Similar noise thresholding has been performed when calculating the delay and Doppler spreads. The noise power is estimated from the regions where no signal is present in the APDPs. Figs. 3(e) and 3(f) show the predicted channel gains obtained from ray-tracing simulations compared with the measurement data as well as with the empirical channel model for both the scenarios.

In Fig. 3(e), a very good agreement is found between measurement, model and simulation results in the LOS region ($t \geq 6.8\,\text{s}$) and in the transition region from NLOS to LOS ($6.8\,\text{s} \geq t \geq 5.7\,\text{s}$). Similarly, in Fig. 3(f), a very good agreement is found between measurement, model and simulation results mainly in the LOS region ($t \geq 7.9\,\text{s}$) and the region $1\,\text{s}$ before the LOS. The most significant power contribution arises from the LOS component and the first order specular and non-specular reflections that are captured by the ray-tracer. There is a noticeable difference of about $8-10\,\text{dB}$ during the NLOS periods ($t \leq 5.7\,\text{s}$) and $6-40\,\text{dB}$ during the NLOS periods

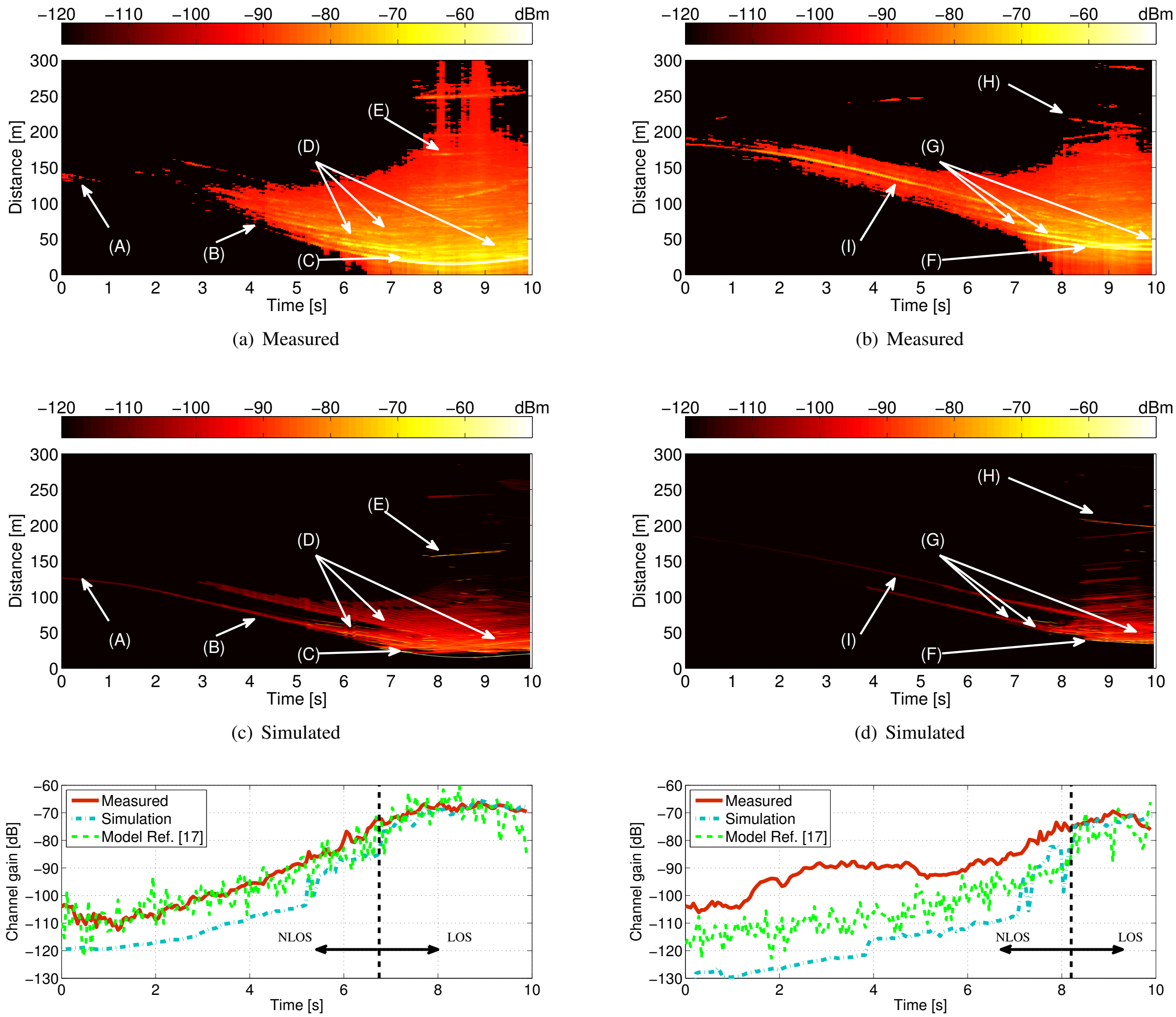

(a) Measured (b) Measured

(c) Simulated (d) Simulated

(e) (f)

Fig. 3. Averaged time-varying power delay profile obtained from the channel sounder data ((a), (b)), the predicted CIRs using the ray-tracing channel model ((c), (d)), and measured versus simulated channel gain compared with an empirical channel model ((e), (f)) from M1 and M2, respectively. The first and second order reflections from the static objects are considered only.

$t \leq 7.9\,\mathrm{s}$) in Fig. 3(e) and Fig. 3(f), respectively. However, the difference in the channel gain between the empirical model and measured is smaller than the difference in the channel gain between the measured and simulation. This is due to the fact that the empirical model is developed based on a large amount of data samples from several different intersections and the model depicts an average channel behavior of the urban intersections. The considered intersection where measurements were taken is slightly special as it has many metallic windows and balconies, which results in a higher received power than usual in the NLOS. For that reason, the empirical model gives better estimates in both the LOS and NLOS, while the simulations provide good estimates only in the LOS situation.

It is evident from the APDPs that in the NLOS situation the ray-tracer underestimates the channel gain. We have found two reasonable explanations for this huge gap in NLOS situations of both scenarios: 1) The buildings in the four corners of the investigated intersections feature a lot of glass or metallic surfaces (e.g. windows and balcony elements) that yield strong power contributions at the receiver caused by specular and non-specular reflections. Especially, in scenario M2 we find a significant reflection (cf. arrow (I) in Fig. 3(b)) that is present even at the beginning of the scenario where both TX and RX are far away from the intersection. The same measurement was analyzed in [17], where the results were compared against a measurement based NLOS pathloss model. It was found that the NLOS model too was unable to capture such a strong reflection coming from metallic surface on the wall which is not typical for NLOS situations in urban intersections. Please note that a similar strong reflection can be identified in scenario M1 (cf. arrow (A) in Fig. 3(a)) which is blocked by earlier mentioned the left-turning bus for $0.5\,\mathrm{s} < t \leq 3\,\mathrm{s}$.

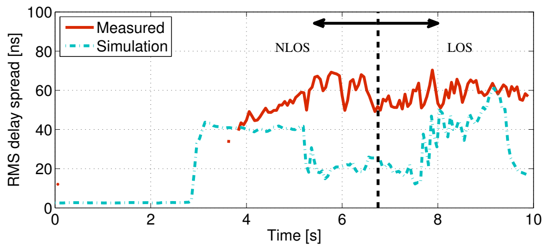

(a)

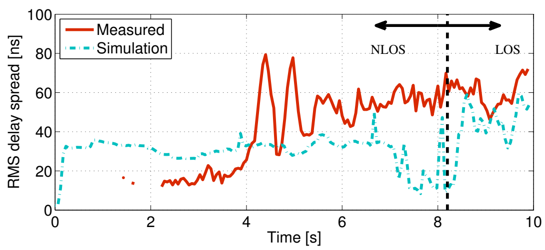

(b)

Fig. 4. Measured versus simulated time-varying RMS delay spread of: (a) M1 - with percentage error of 48.2% in NLOS and 41.5% in LOS, and (b) M2 - with percentage error of 45.2% in NLOS and 39.5% in LOS.

The corresponding MPCs can also be found in the simulation-based PDPs (cf. arrows (B) and (I) in Fig. 3(c) and Fig. 3(d), respectively). However, the ray-tracer treats the walls of the buildings as homogeneous concrete surfaces that explains why the power contribution in the simulations is too small. The inclusion of individual objects, like windows or balconies, with different material parameters requires further implementation efforts, leading to increased computational complexity but of course should also result in better accuracy.

The second reasonable explanation is: 2) The ray-tracer does not capture the effects of higher-order non-specular reflections at all since these phenomena are not implemented in the mathematical model. The metallic and glass elements on the buildings close to the intersection provide good conditions for multi-boucne interactions between the transmitter and receiver. This fact leads to an additional mismatch between measurement and simulation for the investigated intersection.

The results are summarized by presenting the mean error

$$\mu = \mathrm{E}\{\epsilon(t)\} \tag{5}$$

and the standard deviations

$$\sigma = \sqrt{\mathrm{E}\left\{|\mu - \epsilon(t)|^2\right\}} \tag{6}$$

between simulated and measured channel gains where the error ϵ is given by

$$\epsilon(t) = G_{meas}(t) - G_{sim}(t). \tag{7}$$

The values are given in Table I for both the measurements M1 and M2, separately for the LOS and NLOS.

C. Delay and Doppler Spreads

In a multipath propagation environment the signal spreads both in the delay and the Doppler domains. A number of delayed and scaled copies of the transmitted signal arrive at the receiver, and the effect of motion of the TX, RX or scatterers induce frequency and time selective fading that can be characterized by the root mean square (RMS) delay and Doppler spreads, respectively. These measures are inversely proportional to the coherence bandwidth and coherence time of the channel, respectively [27]. The instantaneous RMS delay spread is the normalized second-order central moment of the time-variant PDP $P_\tau(t_k, \tau)$ and is defined as

$$S_\tau(t_k) = \sqrt{\frac{\sum_i P_\tau(t_k, \tau_i)\tau_i^2}{\sum_i P_\tau(t_k, \tau_i)} - \left(\frac{\sum_i P_\tau(t_k, \tau_i)\tau_i}{\sum_i P_\tau(t_k, \tau_i)}\right)^2}. \tag{8}$$

The measured and simulated RMS delay spreads are shown in Fig. 4(a) for M1 and in Fig. 4(b) for M2. For the simulations bandwidth of 240 MHz at 5.6 GHz center frequency was used as it was in the measurements.

The delay spread of the simulated data is mostly smaller than the delay spread of measured data because the number of specular and non-specular MPCs captured by the ray-tracer are much smaller than that of the measurements due to the limited information about the scattering environment. In addition to these missing discrete MPCs, parts of the diffuse scattering that can be observed in the measured PDP with large delays do not appear in the simulations. The mean error and standard deviation are obtained by (5) and (6), respectively, whereas $\epsilon(t)$ refers to the error between the measured and simulated RMS delay spread as a function of time. The values are summarized in Table I. We do not find a reasonable agreement, with a percentage error of around 40% and a mean error of around 24 ns in the LOS and approximately the same in the NLOS situation for both M1 and M2. As a result, we can conclude that a simplified version of the ray-tracing model is not sufficient to provide reliable information about the time-dispersive behavior of the wideband urban channel.

Similarly, the instantaneous RMS Doppler spread is the normalized second-order central moment of the time-variant Doppler spectral density (DSD). The DSD $P_\nu(t_k, \nu)$ at time instants $t_k \ \forall \ k = 0, 1, ..., N_t$ is calculated analogous to PDP by taking the Fourier transform of the impulse response $h(t_k + n\Delta t, \tau) \ \forall \ n = 0, 1, ..., N_{avg}$ in the time domain - $h(t_k + n\Delta t, \tau)$ is a sliding window of N_{avg} time snapshots - and averaged over the delay domain,

$$\mathbf{P}_\nu(t_k, \nu) = \frac{1}{N_\tau} \sum_{m=0}^{N_\tau - 1} |\mathbf{h}(\nu, m\Delta\tau)|^2, \tag{9}$$

where N_τ is the number of delay taps. Averaging over the delay domain is analogous to considering the narrowband CIR $h(t)$ at first place and then calculating the Doppler spectral density by taking Fourier transform in the time domain. The Doppler spread can be computed as

$$S_\nu(t_k) = \sqrt{\frac{\sum_i P_\nu(t_k, \nu_i)\nu_i^2}{\sum_i P_\nu(t_k, \nu_i)} - \left(\frac{\sum_i P_\nu(t_k, \nu_i)\nu_i}{\sum_i P_\nu(t_k, \nu_i)}\right)^2}. \tag{10}$$

The measured and simulated RMS Doppler spreads are shown in Fig. 5(a) for M1 and in Fig. 5(b) for M2. The mean error and

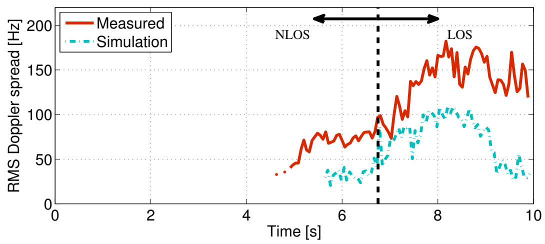

(a)

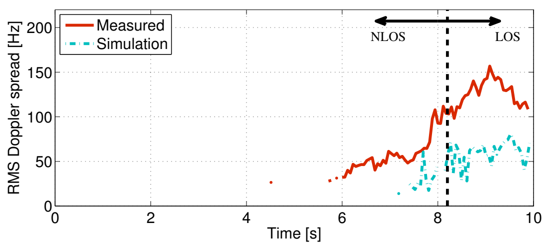

(b)

Fig. 5. Measured versus simulated time-varying RMS Doppler spread of: (a) M1 - with percentage error of 52.4% in NLOS and 47.2% in LOS, and (b) M2 - with percentage error of 62.4% in NLOS and 53.9% in LOS..

standard deviation are obtained by (5) and (6), respectively, whereas $\epsilon(t)$ here refers to the error between the measured and simulated RMS Doppler spread and are summarized in Table I.

As mentioned above, only static objects are considered in the simulations as there were not many moving vehicles present during the measurements. The Doppler spread of the simulated data captures the trend but it is much smaller than that of the measured data for two main reasons. First, the ray-tracing model is able to capture some, but not all, of the significant MPCs because of the known limitations. Second, incomplete building data and incorrect material properties lead to incorrect power level estimates for several MPCs. Implying that the assigned weights to the Doppler shifts associated to those MPCs are incorrect. These limitations in turn result in a smaller Doppler spread even though the trend is similar.

D. Antenna Diversity

Random fluctuations in the signal power due to multipath propagation caused by scattering impair the wireless channel across space, time and frequency. This is commonly known as channel fading. Diversity techniques are developed to combat fading by combining several independently faded version of the same transmitted signal at the receiver to improve link reliability by improving the signal-to-noise ratio (SNR). Thus, diversity gain is an important metric to be analyzed in order to validate the performance of ray-tracing channel simulations for MIMO V2V systems.

Among the diversity techniques, here spacial (or antenna) diversity is of particular interest. In this scheme multiple antennas at the TX and/or RX are used to realize diversity gains. In order to evaluate antenna diversity captured in the ray-tracing simulations we compare two metrics, the eigenvalue distribution and antenna correlation in the following.

1) Eigenvalue distribution and array gain: The eigenvalues (EVs) and their distributions obtained from ray-tracing simulations are compared against the ones obtained from the measurement data as they capture important properties of the array and the medium [28]. An SVD expansion of the normalized channel matrix $\mathbf{H} \in \mathbb{C}^{M_R \times M_T}$ can be written as,

$$\mathbf{H} = \mathbf{U} \cdot \mathbf{S} \cdot \mathbf{V}^*, \tag{11}$$

where $\mathbf{U}$ is an $M_R \times M_R$ unitary matrix, $\mathbf{S}$ is a diagonal matrix of real non-negative singular values σ_m where $m = 1, 2, ..., \min\{M_R, M_T\}$, and $\mathbf{V}^*$ (the conjugate transpose of $\mathbf{V}$) is an $M_T \times M_T$ unitary matrix. Singular values of $\mathbf{H}$ are the square roots of the eigenvalues of $\mathbf{HH}^*$. The matrix H here represents a narrow band channel transfer function, however the SVD is computed over all frequency tones in the 240 MHz bandwidth and then averaged over the whole bandwidth, as the uncorrelated scattering assumption is valid for 240 MHz at 5 GHz band [29].

In Fig. 6(a) and 6(b), the time evolution of the eigenvalues, λ_m where $m = 1, 2, ..., \min\{M_R, M_T\}$, of the measured and simulated data are compared for both M1 and M2. The markers represent measured eigenvalues whereas the lines represent simulated eigenvalues. It is interesting to notice that the eigenvalues of the measured and simulated data are very similar. For the first 5 s in both M1 and M2 the eigenvalues are similar, but the scenario is NLOS and the available signal power is very weak. In such a situation the noise, which is approximately i.i.d. Gaussian in both the measurements as well as in the simulations, dominates. This in turn gives the same eigenvalues. However, in Fig. 6(b) there are some differences in the eigenvalues between $2-5$ s because of the presence of the dominating MPCs in the NLOS in M2 as discussed before. As the eigenvalues deal with the narrow band and singularity properties of the channel, they provide a good agreement even when only a few MPCs are extracted by the simulation, e.g., in the NLOS situation.

In Fig. 6(c)-6(d) the eigenvalues are plotted as a function of channel gain. The eigenvalues are shown only for the samples where the channel gain is higher than -100 dB, for the region in time where the signal dominates the noise. As the ray-tracing simulations do not extract all MPCs and thus provide lower channel gain, we see some gaps in the plots where the eigenvalues correspond to lower channel gain than in reality. The mean and standard deviation of the error in the eigenvalues are listed in Table I.

2) Antenna correlation: Multiple antennas at the TX or at the RX can improve the system performance through diversity arrangements, but their benefits can only be fully utilized if the correlation between signals at different antenna elements is low [30]. Thus, antenna correlation for both the TX and the RX array is an important parameter to study. The time-variant antenna correlation $\rho_{ij}^{RX}(t_k)$ between the RX elements i and j is calculated as

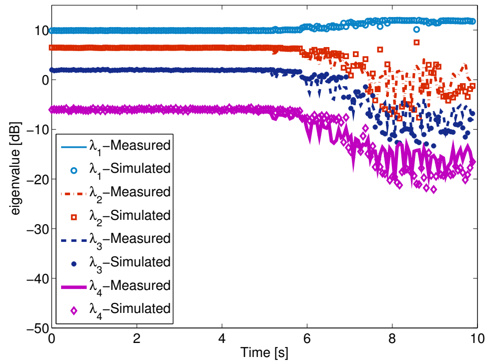

(a)

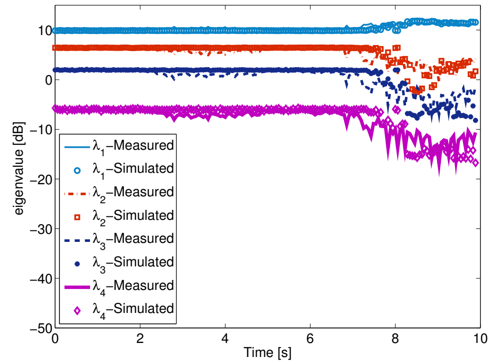

(b)

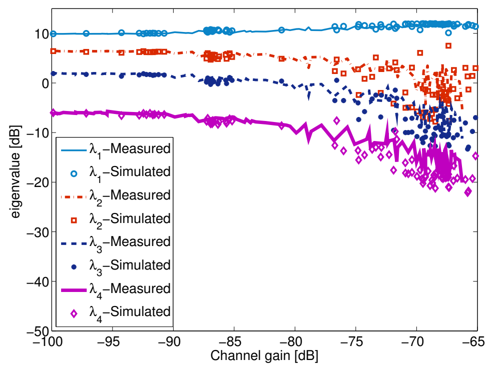

(c)

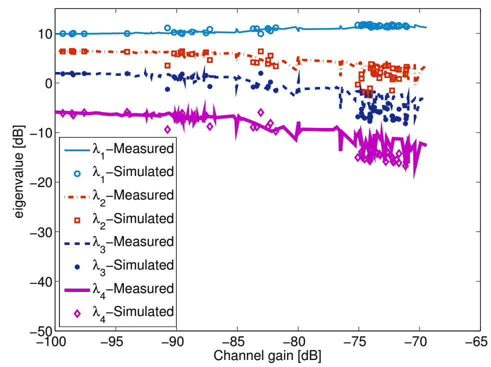

(d)

Fig. 6. Measured versus simulated eigenvalues: Figs. 6(a), and 6(c) represent M1 and Figs. 6(b), and 6(d) represent M2.

TABLE I
MEAN μ AND STANDARD DEVIATION σ OF THE ERROR IN THE ESTIMATED PARAMETERS OBTAINED FROM THE SIMULATED DATA WITH RESPECT TO MEASUREMENT DATA FOR BOTH M1 AND M2.

Parameters		**LOS**		**NLOS**	
		M1	**M2**	**M1**	**M2**
		(μ_1, σ_1)	(μ_2, σ_1)	(μ'_1, σ'_1)	(μ'_2, σ'_1)
Channel gain	G_h [dB]	(0.87, 1.66)	(3.12, 5.43)	(11.2, 2.75)	(26.2, 6)
Delay spread	τ [ns]	(24.5, 13.5)	(23.2, 17.2)	(24, 17.5)	(9.3, 20)
Doppler spread	μ [Hz]	(64.8, 28.9)	(62.7,20.1)	(40.4, 10.2)	(34.4,6.34)
Eigenvalues	λ_1 [dB]	(-0.07, 0.38)	(-0.07, 0.49)	(0.104, 0.19)	(0.28, 0.26)
	λ_2 [dB]	(1.88, 4.26)	(0.92, 2.5)	(-0.21, 0.51)	(-0.49, 0.59)
	λ_3 [dB]	(2.41, 3.36)	(1.55, 3.18)	(-0.37, 0.76)	(-0.69, 0.75)
	λ_4 [dB]	(2.41, 3.1)	(1.08, 3.23)	(-0.52, 0.98)	(-0.77, 0.82)
TX antenna correlations coefficients	ρ_{12}	(-0.31, 0.23)	(-0.31, 0.24)	(-0.032, 0.11)	(0.1, 0.1)
	ρ_{13}	(-0.12, 0.3)	(-0.11, 0.33)	(0.07, 0.108)	(0.117, 0.12)
	ρ_{14}	(-0.12, 0.23)	(-0.14, 0.26)	(0.02, 0.106)	(0.17, 0.13)
	ρ_{23}	(-0.12, 0.17)	(-0.18, 0.27)	(0.1, 0.19)	(0.12, 0.1)
	ρ_{24}	(-0.13, 0.27)	(-0.14, 0.25)	(0.03, 0.12)	(0.17, 0.14)
	ρ_{34}	(0.11, 0.23)	(-0.07, 0.23)	(0.07, 0.14)	(0.21, 0.13)
RX antenna correlations coefficients	ρ_{12}	(-0.22, 0.21)	(-0.27, 0.27)	(0.043, 0.11)	(0.07, 0.09)
	ρ_{13}	(-0.20, 0.33)	(0.02, 0.2)	(-0.002, 0.104)	(0.04, 0.07)
	ρ_{14}	(-0.03, 0.19)	(0.026, 0.15)	(-0.007, 0.08)	(0.06, 0.09)
	ρ_{23}	(-0.18, 0.18)	(-0.17, 0.23)	(0.05, 0.09)	(0.21, 0.16)
	ρ_{24}	(0.008, 0.33)	(-0.21, 0.33)	(0.02, 0.09)	(0.16, 0.15)
	ρ_{34}	(-0.01, 0.16)	(0.03, 0.21)	(-0.01, 0.103)	(0.17, 0.14)

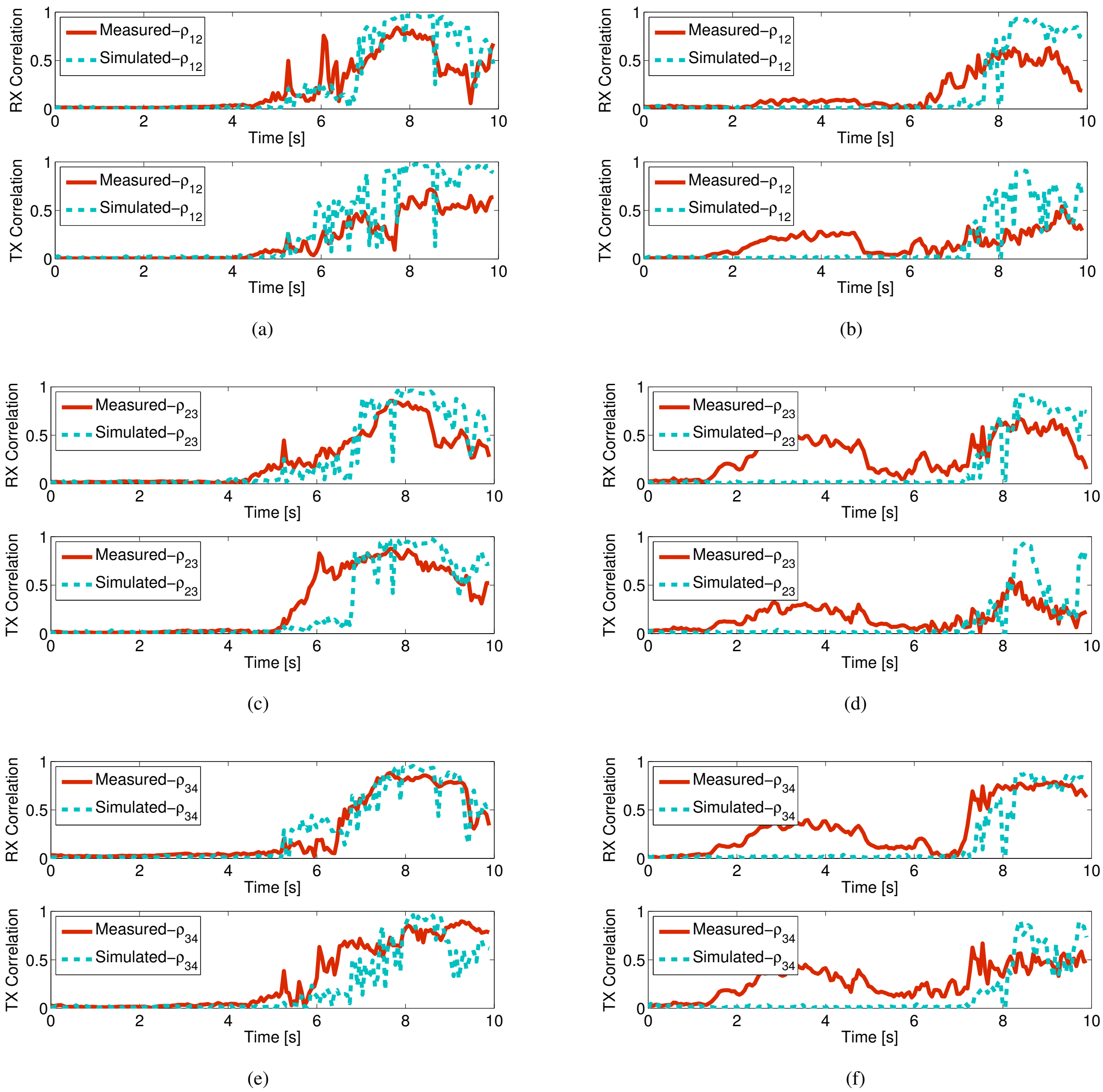

Fig. 7. The correlation between the antenna elements $1-2$, $1-3$, and $1-4$ is shown as a function of time. Figs. 7(a), 7(c), and 7(e) represent M1 and Figs. 7(b), 7(d), and 7(f) represent M2.

$$\rho_{ij}^{RX}(t_k) = \sum_{n_t=1}^{N_{avg}} \sum_{n_f=1}^{N_f} \frac{\sum_{m=1}^{M_T} H_{i,m} H_{j,m}^*}{\sqrt{\sum_{m=1}^{M_T} |H_{i,m}|^2 \sum_{m=1}^{M_T} |H_{j,m}|^2}}. \quad (12)$$

Similarly, the correlation $\rho_{ij}^{TX}(t_k)$ between the TX elements i and j is calculated as,

$$\rho_{ij}^{TX}(t_k) = \sum_{n_t=1}^{N_{avg}} \sum_{n_f=1}^{N_f} \frac{\sum_{n=1}^{M_R} H_{n,i}^* H_{n,j}}{\sqrt{\sum_{n=1}^{M_R} |H_{n,i}|^2 \sum_{n=1}^{M_R} |H_{n,j}|^2}}, \quad (13)$$

where $H_{n,m}$ is a block matrix for each time instant t_k, n^{th} RX and m^{th} TX elements, respectively, such that $H \in \mathbb{C}^{N_{avg} \times N_f}$ and H^* is the conjugate transpose of H. N_f is the number of frequency bins within measurement bandwidth.

In Fig. 7, the correlation between the antenna elements is shown as a function of time. The mean and standard deviation of the error in correlations is listed in Table I. The correlation between the elements is almost zero from $t = 0\,s$ until t reaches approximately 6 s. In this time interval, i.i.d. Gaussian noise is the dominating contribution, which results in mostly uncorrelated subchannels. The correlation between all elements is higher when there is LOS between the TX and RX in both M1 and M2. The antenna correlation coefficients for consecutive antenna elements $1-2$, $2-3$, and $3-4$ of both the RX and TX arrays for M1 are shown in Figs. 7(a), 7(c), and 7(e). The measured and simulated correlation coefficients are not exactly the same but show a similar trend over the time. Similarly, the antenna correlation coefficients for antenna elements $1-2$, $2-3$, and $3-4$ of both the RX and TX arrays for M2 are shown in Figs. 7(b), 7(d), and 7(f). For M2, again the correlation between $2-5\,\mathrm{s}$ is higher for measurement than that in simulations. However, in the presence of LOS the correlation of the TX and RX from the simulation and measurement show similar trend. For the ray-tracing simulations measured polarimetric antenna responses were used for all the antennas of 4x4 MIMO arrays mounted at the TX and RX cars, which is beneficial for the antenna correlation estimation. Moreover, ray-tracer is able to capture and track some of the significant MPCs from the surroundings even though their estimated powers may not be accurate due to incorrect material properties. However for the antenna correlation the spatial signatures of MPCs are more important than their actual powers that in turn helps to capture the trends in the antenna correlation.

VI. Conclusions

The channel characterization of an urban intersection for V2V communication is non-trivial as many difficult to capture details of the environment may have a huge impact on the experienced radio channel. This includes the structure, material, position and alignment of buildings, street width, location and density of roadside objects and so forth. An accurate model is required for safety-critical system design, which in turn requires a full understanding of these physical effects. Deterministic models such as those achieved with a ray-tracer are eventually anticipated as good candidates to model such complex scenarios.

In this paper, we have presented an accuracy analysis of a ray-tracing model with some given limitations, which is used to simulate the V2V channels in an urban intersection scenario. We have compared important channel metrics, namely those of power delay profile, channel gain, delay and Doppler spreads, eigenvalues and antenna correlation that are obtained from ray-tracing based simulations as well as from the channel sounder measurements. Analyzing these metrics, the possible flaws of the underlying propagation models are identified in the two tools and they are evaluated on their accuracy.

The current release of the ray-tracing model constitutes a good basis to characterize the narrowband urban V2X radio channel, especially in LOS scenario. We have identified limitations of the ray-tracing model when modeling the wideband characteristics of channel. The analysis presented here has revealed that multi-bounce non-specular reflections and diffuse scattering causes considerable power contributions in the urban NLOS scenario. Thus, implementation of propagation mechanisms such as (i) higher order reflections (ii) diffuse scattering and (iii) diffraction from the corners of houses or large vehicles are required in the model to improve the accuracy of the ray-tracing algorithm. In this work, we have been interested to use a simplified ray-tracing model for reasons of complexity and likewise an extension of the of the ray-tracing routine to capture these effects remains for future work.

Through the direct comparison of channel sounding data and ray-tracing simulations of a specific V2X scenario we provide enlightening insights of which propagation effects cannot be neglected when modeling a V2X intersection scenario. Based on the results obtained from this analysis the main goal of the authors is to develop a robust and flexible propagation model in future for the analysis of an arbitrary V2X intersection scenario. Such a model can be integrated into network simulators of other research groups and provides better approximation of a deterministic channel characterization in safety-critical urban traffic scenarios. The end-goal is to enable cost-efficient and flexible simulation of realistic vehicular communication scenarios, which will be an important driver for the worldwide development of future V2X applications.

Acknowledgment

This work has been carried out in close collaboration between Lund University and TU Braunschweig within the COST IC 1004 framework. The authors would like to thank the IC 1004 committee for supporting and funding this short-term scientific mission that was hosted by the Institut für Nachrichtentechnik, Technische Universität Braunschweig, Braunschweig, Germany. We would also like to thank Delphi Deutschland GmbH, Bad Salzdetfurth, Germany for their contribution to the measurement campaign.

References

[1] W. Wiesbeck and S. Knorzer, “Characteristics of the mobile channel for high velocities,” in *Electromagnetics in Advanced Applications, 2007. ICEAA 2007. International Conference on*, 2007, pp. 116–120.

[2] A. F. Molisch, F. Tufvesson, J. Karedal, and C. F. Mecklenbräuker, “A survey on vehicle-to-vehicle propagation channels,” in *IEEE Wireless Commun. Mag.*, vol. 16, no. 6, 2009, pp. 12–22.

[3] I. Sen and D. W. Matolak, “Vehicle-vehicle channel models for the 5 GHz band,” *IEEE Trans. Intell. Transp. Syst.*, vol. 9, no. 2, pp. 235–245, Jun. 2008.

[4] A. Paier, L. Bernado, J. Karedal, O. Klemp, and A. Kwoczek, “Overview of vehicle-to-vehicle radio channel measurements for collision avoidance applications,” in *Vehicular Technology Conference (VTC 2010-Spring), IEEE 71st, Taipei, Taiwan*, May 2010, pp. 1–5.

[5] J. Nuckelt, M. Schack, and T. Kürner, “Deterministic and stochastic channel models implemented in a physical layer simulator for Car-to-X communications,” *Advances in Radio Science*, vol. 9, pp. 165–171, Sept. 2011.

[6] T. Mangel, O. Klemp, and H. Hartenstein, “5.9 GHz inter-vehicle communication at intersections: a validated non-line-of-sight path-loss and fading model,” *EURASIP Journal on Wireless Communications and Networking*, vol. 2011, no. 1, p. 182, 2011.

[7] C. Sommer, D. Eckhoff, R. German, and F. Dressler, “A computationally inexpensive empirical model of IEEE 802.11p radio shadowing in urban environments,” in *Wireless On-Demand Network Systems and Services (WONS), 2011 Eighth International Conference on*, 2011, pp. 84–90.

[8] S. Hosseini Tabatabaei, M. Fleury, N. Qadri, and M. Ghanbari, “Improving propagation modeling in urban environments for vehicular ad hoc networks,” *Intelligent Transportation Systems, IEEE Transactions on*, vol. 12, no. 3, pp. 705–716, 2011.

[9] T. Gaugel, L. Reichardt, J. Mittag, T. Zwick, and H. Hartenstein, “Accurate simulation of wireless vehicular networks based on ray tracing and physical layer simulation,” in *High Performance Computing in Science and Engineering ’11*. Springer Berlin Heidelberg, 2012, pp. 619–630.

[10] A. Chelli and M. Patzold, “The impact of fixed and moving scatterers on the statistics of MIMO vehicle-to-vehicle channels,” in *Vehicular Technology Conference, 2009. VTC Spring 2009. IEEE 69th*, 2009, pp. 1–6.

[11] A. Zajic and G. Stuber, “Three-dimensional modeling and simulation of wideband mimo mobile-to-mobile channels,” *Wireless Communications, IEEE Transactions on*, vol. 8, no. 3, pp. 1260–1275, 2009.

[12] R. Santos, A. Edwards, and V. Rangel-Licea, *Wireless Technologies in Vehicular Ad Hoc Networks: Present and Future Challenges*. Hershey, PA: IGI Global (701 E. Chocolate Avenue, Hershey, Pennsylvania, 17033, USA), 2012.

[13] J. Maurer, T. Fugen, T. Schafer, and W. Wiesbeck, “A new inter-vehicle communications (IVC) channel model,” in *Vehicular Technology Conference, 2004. VTC2004-Fall. 2004 IEEE 60th*, vol. 1, 2004, pp. 9–13 Vol. 1.

[14] J. Nuckelt, T. Abbas, F. Tufvesson, C. F. Mecklenbräuker, L. Bernado, and T. Kürner, “Comparison of ray tracing and channel-sounder measurements for vehicular communications,” in *2013 IEEE 77th Vehicular Technology Conference: VTC2013-Spring, Dresden, Germany*, June 2013, pp. 1–5.

[15] Google earth v7.1.1.1888 (2013). [Online]. Available: http://www.google.com/earth/index.html [Accessed: 2013/08/15]

[16] M. Schack, J. Nuckelt, R. Geise, L. Thiele, and T. Kürner, “Comparison of path loss measurements and predictions at urban crossroads for C2C communications,” in *5th European Conference on Antennas and Propagation (EuCAP), Rome, Italy*, April 2011.

[17] T. Abbas, A. Thiel, T. Zemen, C. F. Mecklenbräuker, and F. Tufvesson, “Validation of a non-line-of-sight path-loss model for V2V communications at street intersections,” in *13th International Conference on ITS Telecommunications, Tampere, Finland*. IEEE, November 2013.

[18] J. Karedal, F. Tufvesson, T. Abbas, O. Klemp, A. Paier, L. Bernadó, and A. F. Molisch, “Radio channel measurements at street intersections for vehicle-to-vehicle safety applications,” in *IEEE VTC 71st Vehicular Technology Conference (VTC 2010-spring), Taipei, Taiwan*, May 2010, pp. 1–5.

[19] A. Thiel, O. Klemp, A. Paier, L. Bernadó, J. Karedal, and A. Kwoczek, “In-situ vehicular antenna integration and design aspects for vehicle-to-vehicle communications,” in *Antennas and Propagation (EuCAP), 2010 Proceedings of the Fourth European Conference on, Barcelona, Spain*, Apr. 2010, pp. 1–5.

[20] J. McKown and J. Hamilton, R.L., “Ray tracing as a design tool for radio networks,” *IEEE Network*, vol. 5, no. 6, pp. 27–30, 1991.

[21] M. Schack, “Integrated simulation of communication applications in vehicular environments,” Ph.D. dissertation, Technische Universität Braunschweig, 2013.

[22] V. Degli-Esposti, “A diffuse scattering model for urban propagation prediction,” *Antennas and Propagation, IEEE Transactions on*, vol. 49, no. 7, pp. 1111–1113, Jul 2001.

[23] M. Boban, J. Barros, and O. K. Tonguz, “Geometry-based vehicle-to-vehicle channel modeling for large-scale simulation,” *CoRR*, vol. abs/1305.0124, 2013.

[24] J. Nuckelt, D. Rose, T. Jansen, and T. Kurner, “On the use of openstreetmap data for v2x channel modeling in urban scenarios,” in *Antennas and Propagation (EuCAP), 2013 7th European Conference on*, 2013, pp. 3984–3988.

[25] J. Nuckelt, M. Schack, and T. Krner, “Geometry-based path interpolation for rapid ray-optical modeling of vehicular channels,” in *9th European Conference on Antennas and Propagation (EuCAP)*, 2015.

[26] Z. Li, R. Wang, and A. Molisch, “Shadowing in urban environments with microcellular or peer-to-peer links,” in *Antennas and Propagation (EUCAP), 2012 6th European Conference on*, 2012, pp. 44–48.

[27] A. Molisch and M. Steinbauer, “Condensed parameters for characterizing wideband mobile radio channels,” *International Journal of Wireless Information Networks*, vol. 6, no. 3, pp. 133–154, 1999.

[28] R. Vaughan and J. B. Andersen, *Channels, Propagation and Antennas for Mobile Communications (IEE Electromagnetic Waves Series, 50)*. Institution of Engineering and Technology, Feb. 2003.

[29] L. Bernadó, T. Zemen, F. Tufvesson, A. F. Molisch, and C. F. Mecklenbräuker, “Delay and doppler spreads of non-stationary vehicular channels for safety relevant scenarios,” *CoRR*, vol. abs/1305.3376, 2013.

[30] A. Molisch, *Wireless Communications*. Chichester, West Sussex, UK: IEEE Press-Wiley, 2005.

Taimoor Abbas (S09, M14) received his M.Sc. degree in Electronics from Quaid-i-Azam University Islamabad in 2006, and M.S. degree in wireless Communications and Ph.D. degree in radio systems from the department of Electrical and Information Technology, Lund University in 2009 and 2014, respectively. He has been with Ericsson (2008-2009) for his master thesis internship. Currently he is a consultant in Network Design group at Volvo Cars Corporation. His research interests include estimation and modeling of radio channels for vehicle-to-vehicle (V2V) and vehicle-to-infrastructure (V2I) communications, 5G and multi-antenna systems.

Jörg Nuckelt Jörg Nuckelt received the Diploma in electrical engineering from University of Applied Sciences Zittau/Görlitz, Zittau, Germany, in 2007. In 2009 and 2014, he received the M.Sc. degree and the Ph.D. degree both in electrical engineering from the Technische Universität Braunschweig, Braunschweig, Germany. He is interested in wireless communications, channel modeling and physical layer topics related to vehicular communication networks. He joined Siemens AG in 2015, where he is now working in the area of communication-based train control.

Thomas Kürner received the Dipl. Ing. degree in electrical engineering and the Dr.-Ing. degree from Universitaet Karlsruhe, Germany, in 1990 and 1993, respectively. From 1990 to 1994, he was with the Institut fuer Hoechstfrequenztechnik und Elektronik (IHE), Universitaet Karlsruhe, working on wave propagation modeling, radio channel characterization and radio network planning. From 1994 to 2003, he was with the Radio Network Planning Department at the headquarters of the GSM 1800 and UMTS operator E-Plus Mobilfunk GmbH Co KG, Duesseldorf, where he was Team Manager responsible for radio network planning tools, algorithms, processes and parameters. Since 2003, he has been a Full Professor of mobile radio systems at the Institut fuer Nachrichtentechnik (IfN), Technische Universitaet Braunschweig. His working areas are propagation, traffic and mobility models for automatic planning of mobile radio networks, planning of hybrid networks, car-to-car communications as well as indoor channel characterization for high-speed short-range systems including future terahertz communication systems. He has been engaged in several international bodies such as ITU-R SG 3, UMTS Forum Spectrum Aspects Group and COST 231/273/259/2100. Prof. Dr.-Ing. Krner has been a participant in the European projects ISTMOMENTUM and ICT-SOCRATES. Currently, he is chairing IEEE802.15 IG THz. He has served as Vice-Chair Propagation at the European Conference on Antennas and Propagation (EuCAP), in 2007 and 2009, and has been an Associate Editor of the IEEE TRANSACTIONS ON VEHICULAR TECHNOLOGY since 2008. He is a member of VDE/ITG, VDI, and an elected member of the International Scientific Radio Union (URSI/USNC) Commission F (Radio Wave Propagation and Remote Sensing).

Thomas Zemen (S03, M05, SM10) received the Dipl.-Ing. degree (with distinction) in electrical engineering in 1998, the doctoral degree (with distinction) in 2004 and the Venia Docendi (Habilitation) for ”Mobile Communications” in 2013, all from Vienna University of Technology. Since 2014 Thomas Zemen has been Senior Scientist at AIT Austrian Institute of Technology. From 2003 to 2014 he was with FTW Forschungszentrum Telekommunikation Wien and Head of the ”Signal and Information Processing” department since 2008. From 1998 to 2003 Thomas Zemen worked as Hardware Engineer and Project Manager for the Radio Communication Devices Department, Siemens Austria. He is the author or coauthor of four books chapters, 23 journal papers and more than 70 conference communications. His research interests focuses on ultra-reliable, low-latency wireless machine-to-machine communications for sensor and actuator networks, vehicular channel measurements and modeling, time-variant channel estimation, cooperative communication systems and interference management. Dr. Zemen is docent at the Vienna University of Technology and serves as Associate Editor for the IEEE Transactions on Wireless Communications.

Christoph Mecklenbräuker received the Dipl.-Ing. degree (with distinction) in electrical engineering from Vienna University of Technology, Vienna, Austria, in 1992 and the Dr.-Ing. degree (with distinction) from Ruhr University Bochum, Bochum, Germany, in 1998. From 1997 to 2000, he was with Siemens, Vienna. From 2000 to 2006, he has held a senior research position with Telecommunications Research Center Vienna (FTW) in the field of mobile communications. In 2006, he joined, as a Full Professor, the Faculty of Electrical Engineering and Information Technology, Vienna University of Technology. Since 2009, he has been leading the Christian Doppler Laboratory for Wireless Technologies for Sustainable Mobility, Vienna University of Technology. He was a Delegate to the Third-Generation Partnership Project and was engaged in the standardization of the radio access network for the Universal Mobile Telecommunications System. He is the author of approximately 100 papers in international journals and conferences, for which he has also served as a Reviewer. He is the holder of eight patents in the field of mobile cellular networks. His current research interests include vehicular connectivity, ultrawideband radio, and multiple-inputmultiple-output techniques for wireless systems. Dr. Mecklenbruker is a member of the IEEE Signal Processing, Antennas and Propagation, and Vehicular Technology Societies; the Association for Electrical, Electronic, and Information Technologies, and the European Association for Signal Processing. His doctoral dissertation on matched field processing received the Gert Massenberg Prize in 1998.

Fredrik Tufvesson received his Ph.D. in 2000 from Lund University in Sweden. After two years at a start-up company, he joined the department of Electrical and Information Technology at Lund University, where he is now professor of radio systems. His main research interests are channel modeling, measurements and characterization for wireless communication, with applications in various areas such as massive MIMO, UWB, mm wave communication, distributed antenna systems, vehicular communication systems and radio based positioning. Fredrik is managing the wireless propagation group at the department and has authored and co-authored around 50 journal papers and 110 conference papers.